REPUBLIC OF UGANDA
Ministry of Energy and
Mineral Development
MEMD
Kampala

FEDERAL REPUBLIC OF
GERMANY
Federal Institute for
Geosciences and Natural Resources
BGR
Hannover

TECHNICAL COOPERATION

PROJECT NO.: 2002.2061.1

GEOTHERM Project:

Detailed surface analysis of the Buranga geothermal prospect, West-Uganda

Seismological data analysis, earthquake localization and travel-time tomography

Report

University of Frankfurt

JOHANN WOLFGANG GOETHE
UNIVERSITÄT
FRANKFURT AM MAIN

Frankfurt am Main
2007

Seismological data analysis, earthquake localization and travel-time tomography

by

G. Rümpker, M. Lindenfeld, A. Yakovlev
Section of Geophysics, Institute for Geosciences, University of Frankfurt

Preamble

The Ministry of Energy and Mineral Development (MEMD) through the Geological Survey and Mines Department (GSMD), Uganda, and the Federal Institute for Geosciences and Natural Resources (BGR), Germany, initiated a project with the title “Detailed surface analysis of the Buranga geothermal prospect, West-Uganda” which started in the end 2004.

The project in Uganda is part of the GEOTHERM programme, a technical cooperation programme of the German government. It promotes the use of geothermal energy in partner countries, by kicking off development at promising sites. It supports various countries worldwide, particularly in regions with high geothermal potential. East Africa is the major regional focus of the programme. BGR on behalf of the Federal Ministry for Economic Cooperation and Development (BMZ) started the programme in 2003.

The objective of the GEOTHERM project in Uganda is to raise the development status of Buranga geothermal prospect by geoscientific investigations to reach a pre-feasibility status in the future which is the base for planning of exploration wells. In the beginning of 2005 geological studies, geochemical sampling and geophysical measurements (resistivity methods, gravimetry and seismology) were carried out. Geochemical findings proofed the existence of a magmatic body that most likely serves as the heat source of the hot springs. Hence the task of geophysical measurements was the detection and delineation of this magmatic intrusion. The high seismicity of the region provides excellent conditions for the application of seismological methods. The seismological measurements continued until August 2006.

The University of Frankfurt was commissioned by BGR to undertake detailed analysis of the seismological measurements in the Buranga region that were carried out within the GEOTHERM project. This report describes in detail the data processing, earthquake localization and seismological tomography. Parts of this report will be included in the final report of the GEOTHERM project.

Data processing and preliminary earthquake localization

Deployment of the seismological equipment in the Buranga region to record local earthquakes began in May 2005 with three seismological stations only (**Fig. 1**: Stations NTAN, KARU, ITOJ).

These three stations were operated from May to December 2005. The initial analysis of the recordings documented the very high seismicity of that area (more than 300 local earthquakes per month), demonstrating that Buranga provides excellent conditions for the application of passive seismological methods. Therefore it was decided to deploy more stations: 9 stations were operated since January 2006, 15 stations since April 2006. The data recording finished by the end of August 2006.

The station array covers an area of about 30 times 40 km; the distances between neighbouring stations vary between about 3 and 12 km. Note that the Sempaya hot springs are marginally located at the north-western boundary of the array. A more central location of the target area with respect to the array would have been desirable but a secure operation of seismic stations to the north-west of the hot springs was not possible.

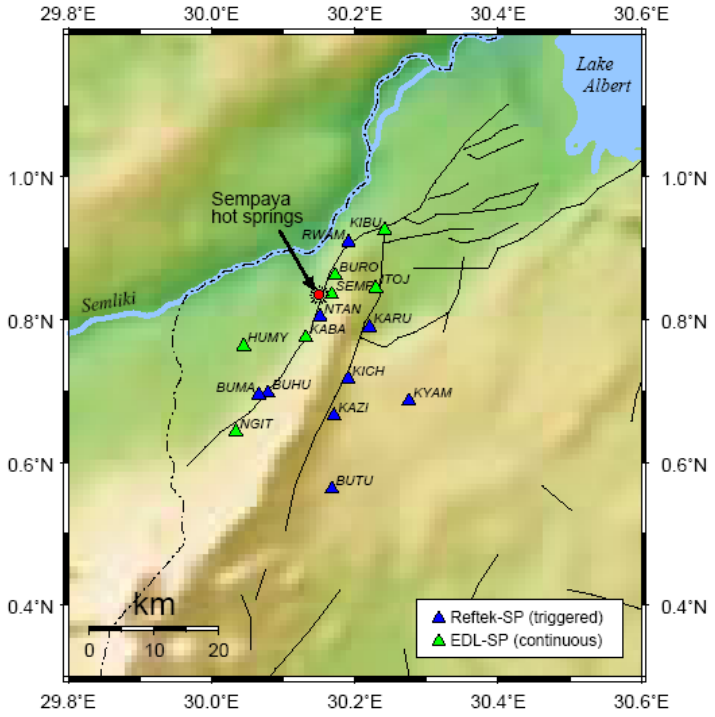

Figure 1. *Map showing the distribution of stations. Note, when the project started in April 2005 only 3 sites were occupied. During the following months the number of stations was gradually increased to 15.*

The data set

Until April 2006 only Reftek data loggers were available for the project. The Reftek data loggers were operated in triggered mode; after this 7 more stations equipped with Earth Data Loggers (EDL) were deployed which were operated in continuous mode. Short period 1 Hz seismometers of type Mark L-4 3D were used at all stations. (The seismological equipment was kindly provided by GFZ Potsdam). The times of operation for each station of the Buranga network are given in **Fig. 2**.

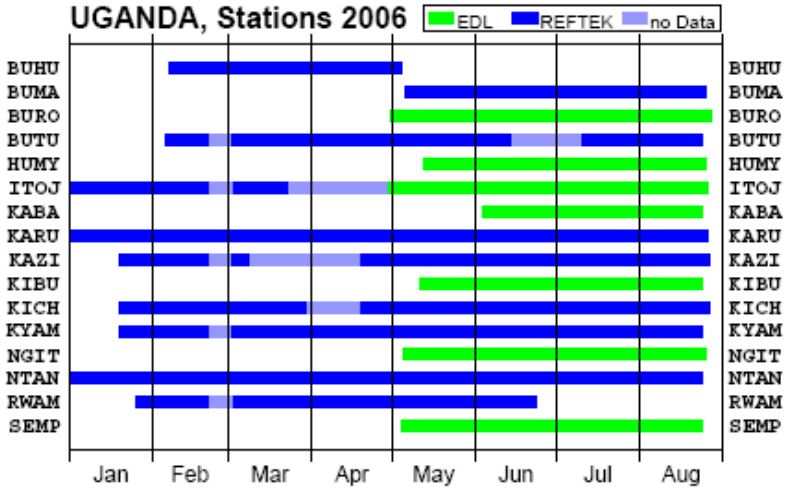

Figure 2. *Times of operation for stations of the Buranga network during 2006.*

As part of this workpackage, the Reftek (Reftek format) and EDL (mini-seed format) data was converted into the SEISAN data format which can be used by the standard SEISAN program for earthquake analysis and event localization (the software is available free of charge at the University of Bergen, Earth Science department, http://www.geo.uib.no/seismo/-software/software.html).

The Reftek triggered data are used as a basis to identify suitable events for further analysis and to select time windows from the EDL continuous data stream. Before standard event-

localization routines can be applied, the picking of P and S wave arrival times is a necessary and time consuming step. For most events, both, local P- and S-wave arrival times were determined.

In total, **49721** phase readings (P- and S-wave arrival times), corresponding to **4185** events, were determined. On average, more than 500 events per month were included in the analysis.

Preliminary localization of hypocenters

The program HYPOCENTER (Lienert et al., 1986; Lienert & Havskov, 1995), as part of the Seisan package, is used for hypocenter localization. The 1-D velocity model used for the initial determination of hypocenters is given in **Tab. 1**. We use P-velocities that are slightly faster than those of the IASPEI standard earth model (Kennett, 1991). A constant P/S-velocity ratio of 1.74 is assumed. Tests reveal that moderate changes of the initial velocity model do not have significant effects of the results of the 3-D tomographic velocity inversion described below.

Depth (km)	Vp (km/s)	Vs (km/s)
0.0	6.2	3.6
12.0	6.6	3.8
23.0	7.1	4.1
31.0	8.05	4.63
50.0	8.25	4.71
80.0	8.5	4.9

***Table 1**: Velocity model used for the initial determination of hypocenters.*

While the 1-D velocity model gives a first impression of the location of hypocenters, it certainly represents the true velocity variations insufficiently. Seismic event locations based on regional 1-D velocity-depth sections can have bias errors caused by travel-time variations within different tectonic provinces and due to ray-paths crossing boundaries between tectonic provinces with different crustal and upper mantle velocity structures. The Rwenzori mountain range is characterized by gneisses of relatively high velocity, whereas the neighbouring regions to the North and West are characterized by slower sedimentary layers that fill the rift graben (Schlüter, 2006).

A velocity model with relatively high values of P-wave velocity (6.2 km/s) close to the surface was used for the localization of hypocenters. While this 1-D model probably represents a valid approximation for the eastern section of the region of interest, the velocities in the western section are likely overestimated. It is noted here, that a highly improved localization of the seismic events as well as a 3-D velocity model will result from the application of the tomographic inversion (see workpackage 2).

Fig. 3 shows locations of earthquakes that have been recorded during the operation of the network. The stations are marked as triangles. The majority of events exhibit a focal depth between 10 and 30 km; the deepest events occur at depths of about 55 km.

For most events, the error of localizations is in the order of about 2-3 km. 80% of all hypocenters exhibit localization errors that are smaller than 5 km. The source-time error for most events is smaller than 0.4 sec. About 80 % of events exhibit a source time error smaller than 0.8 sec.

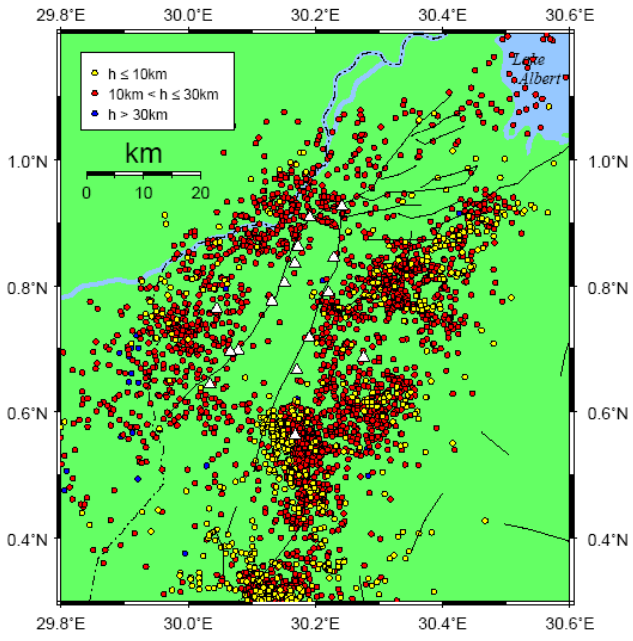

***Figure 3.** Results of the preliminary determination of hypocenters (**4185**) based on the 1-D velocity model given in Table 1. Stations are marked by triangles. Different colours of epicenters indicate different focal depths. Black solid lines indicate locations of surface faults.*

Comparison with mapped near-surface faults

Obviously, few earthquakes occur within the northern part of the Rwenzori block; most events occur outside of the surface expressions of the main marginal faults, the Bwamba fault (west) and the Ruimi-Wasa fault (east), as indicated by the black solid lines in **Fig. 3** The surface locations of faults were obtained from P. Barbirye (2006, pers. comm.).

Events lining the flanks of the Rwenzori range are connected by earthquakes along an east-west trending line near 0.6N, thus separating the northern and southern blocks of the Rwenzori range. This is in agreement with observations by Maasha (1975). Further to the south, most earthquakes are located to the east of the mountains.

From **Fig. 3**, there is no obvious strong correlation between the surface expressions of known faults and epicentre locations. The events seem to be arranged in clustered form and relatively diffuse rather than along linear structures. In part this may be due to the relatively large error ($\approx \pm 3$ km) in locating events which occur outside of the array of stations. However, before a more detailed analysis of hypocenters can take place we first continue with the tomographic inversion of the travel-time residuals and the derivation of a 3-D velocity model

Active-faults and traveltime tomography

A tomographic inversion of the travel-time data was performed to determine the three-dimensional (3-D) structure of the P-and S-wave velocity of the crust beneath the network of stations. The method of travel-time inversion for local earthquakes used here is based on recent developments by Koulakov & Sobolev (2007) and Yakovlev et al. (2007).

The initial velocity model for the tomographic inversion is the same as the 1-D velocity model used for the preliminary localization of hypocenters (**Table 1**). A total number of **2051** events were included in the inversion. This is about half of the total number of events (4185) recorded and identified during the operation of the network. The reduction results in part from the requirement that only those events are used for the inversion for which at least 8 phase readings were determined. This means that each event was recorded by at least 4 stations if both, P and S-wave arrival times were identified. The inversion includes **28644** rays (14445 P-rays and 14199 S-rays) resulting in an average number of about 14 phase readings per event. A further requirement is that the distance between the epicentre and the centre of the array should be less than about 110 km. This is to exclude distant events for which the localization error is relatively large.

In the course of the tomographic inversion (during each step of the iteration) a 3-D velocity model is derived first. Then, on the basis of the improved velocity model, the earthquake hypocenters are re-calculated. The iteration procedure ends when the difference between the new and the previous results becomes insignificant.

Re-localization of earthquakes

In **Fig. 4**, we show hypocenters before and after re-localization. One obvious effect of the re-localization is the stronger clustering of events near, for example, station BUTU or northeast of station KYAM. Events to the west of the Rwenzori range have shifted slightly to the west, now following the course of the Semliki river more closely. This may indicate that the river itself follows the surface expression of an active fault. After re-localization, there exists an almost aseismic area to the west of stations SEMP, NTAN, KABA - close to the location of the hot springs. Furthermore, shallow and deep events near station BUTU are more consistently separated after re-localization. This indicates that these events correspond to a dipping active fault plane, striking north-south.

(a) initial distribution of events

(b) after tomographic inversion and re-localization

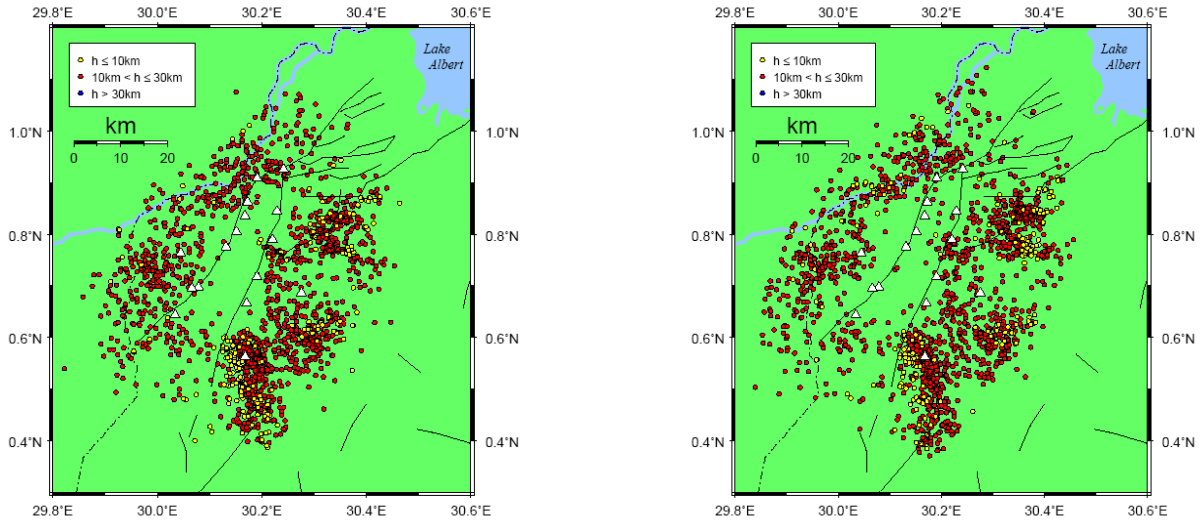

Figure 4. *The re-localization of epicentres (circles) after tomographic inversion. Different colours of epicentres indicate focal depths. Stations are marked by white triangles.*

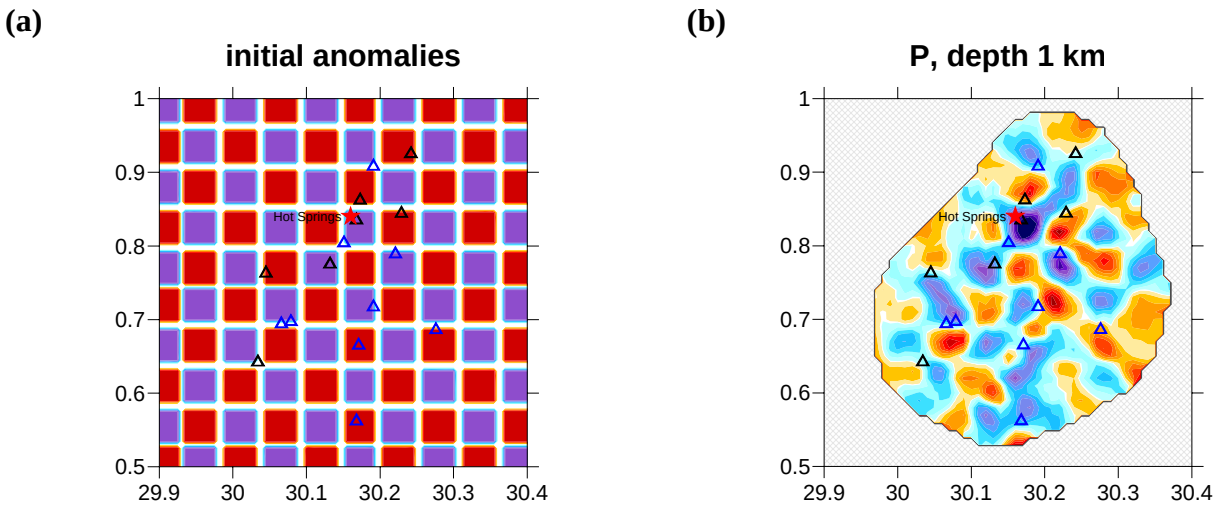

Figure 5. ***(a)*** *Predefined distribution of velocity anomalies for the checker board test. The cell size is5x5 km. Positive (fast) velocity anomalies are marked blue, negative (slow) are marked red.* ***(b)*** *The results of the tomographic inversion of P-wave travel-time residuals.*

Resolution tests (Checker-board tests)

Before the results of the tomographic inversion can be fully appreciated it is important to investigate the resolving power of the given configuration of stations and hypocenters used in the experiment. A related question concerns the size of the anomalies that can be resolved with confidence. In general, velocity structures within an array of stations can be resolved with greater confidence than velocity structures on the outside. The question of resolvability becomes critical as the target area (the hot springs) is located right at the margin of the region covered by the array.

In order to put constraints on the resolution of the tomographic inversion we performed a number of synthetic tests, where theoretical travel times are computed along rays which are traced in a predefined 3-D velocity model (**Fig. 5a**). The distribution of earthquakes and stations is identical to those in the real experiment. Random noise was added to the calculated travel-times to simulate the effects of complex velocity structure and/or errors in the determination of arrival times. The parameters for the tests are: cell size of velocity anomalies: 5x5 km; separation between cells: 1.5 km; amplitude of the anomalies: ±7%; relative noise: 30% of average travel-time residual; relative number of outliers: 5%.

The results of these test show that velocity anomalies within the area covered by the stations can be resolved with confidence. The resolution deteriorates in the peripheral regions. However, near the area of the hot springs, the resolution is relatively good and the shape of the fast and slow velocity anomalies are recovered (approximately) by the inversion (**Fig. 5b**). Regions, were the resolution breaks down, are excluded from the analysis. Further tests also reveal that smaller-scale (< 5 km) anomalies become more difficult to resolve, whereas larger anomalies can be recovered well.

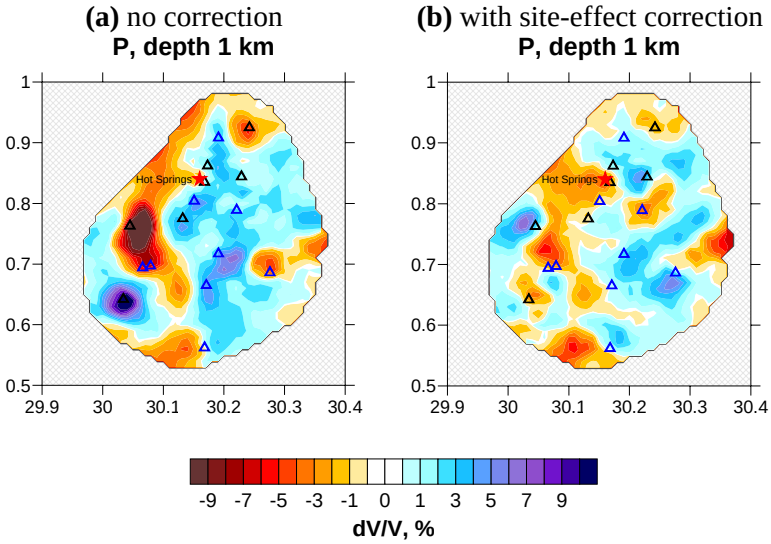

Figure 6. *Example of horizontal section of P-wave velocity anomalies at a depth of 1 km.* ***(a)*** *Result of the direct tomographic inversion.* ***(b)*** *Results after correcting for site effects at isolated stations at the margin of the array.*

Site effects

A further complication arises for relatively isolated stations located at the margin of the array. After inversion of the real data set, relatively large isolated velocity anomalies are found beneath stations HUMY, KIBU, KYAM, and BUTU (**Fig. 6a**). These effects are likely due to very shallow fast and slow velocity anomalies directly beneath the stations. However, as these stations are somewhat separated from the main array, the exact localization of the anomalies is not possible. During the inversion the highly-localized anomalies are smeared out and projected along the ray path into deeper regions (1 km), thus, spoiling the true picture of fast and slow anomalies at depths. We eliminate this effect by explicitly accounting for appropriate correction terms when assigning the travel-time residuals for the stations (**Fig. 6b**).

Detailed analysis of the velocity structure

The tomographic inversion results in refined earthquake locations as well as in 3-D velocity perturbations with respect to the initial 1-D model. An example for a horizontal section of P- and S-wave velocity anomalies at a depth of 1 km is given in **Fig. 7**. Detailed results for additional depths and for P- and S-wave anomalies are given in the appendix **Fig A1**. Generally, the P-wave results may be considered more reliable due to larger uncertainties in the determination of S-wave arrival times.

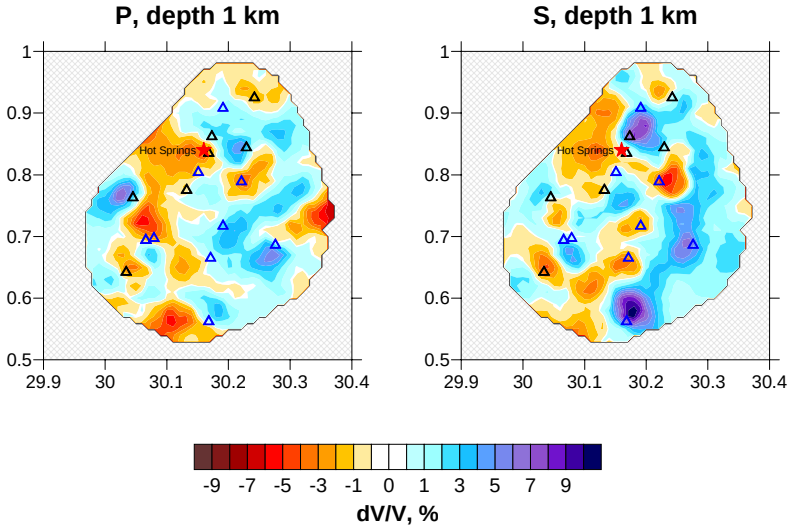

Figure 7. *An example of horizontal sections of P-wave and S-wave velocity anomalies at a depth of 1 km. Additional sections are given in the appendix (**Fig. A1**)*

At shallow depth (1-3 km) the results show that a large low-velocity anomaly exists in the north-western section of the region under investigation. It is interesting to note that the Sempaya hot springs are located at the boundary of this anomaly at the transition between slow and fast regions. The low-velocity anomaly broadens at greater depths (> 5 km). This is similarly seen in the vertical tomographic sections shown in **Fig. 9** and **Fig. A2**. The faster velocities to the east of the hot springs are located beneath the northern block of the Rwenzori range.

A smaller, well resolved, low-velocity anomaly is found near the eastern station of KARU. The anomalies appear to remain separated down to a depth of about 7.5 km. To the south some additional individual anomalies can be found. They merge to a large, more centrally-located, low-velocity anomaly at a depth of about 10 km.

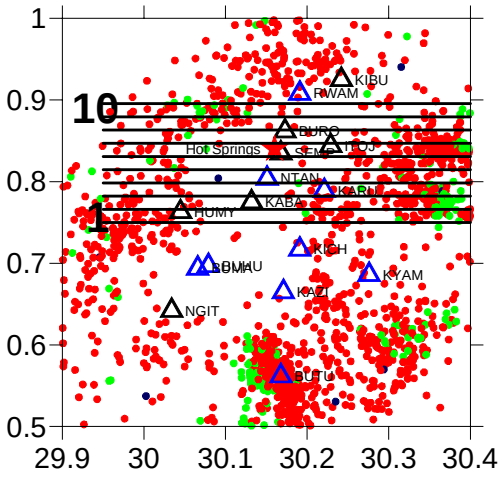

Figure 8. *Positions of vertical sections for which velocity anomalies are shown in **Fig. 9** and **Fig. A2** (see appendix).*

Conclusions

In relation to the location of the hot springs there are several interesting observations that can be derived from this survey. The hot springs are located above the boundary between relatively slow and fast regions in the crust at depth range between 0 and 7 km. The low velocity anomaly broadens beneath this depth range and connects with other smaller anomalies to the east and south. Also, the region to the west/south-west of the hot springs is almost aseismic and it coincides with a low velocity anomaly in the crust (**Fig. 4** and **Fig. 7**).

Geochemical results, from carbon isotopic composition of CO_2, indicate a mantle source for the gas released at the Buranga/Sempaya hot springs. This was confirmed by He isotopic analyses indicating a contribution of >30% mantle He. These findings may imply that a hot actively degassing magma body exists in the subsurface of Buranga area, which may serve as a heat source of the hot springs (Ochmann et al., 2007).

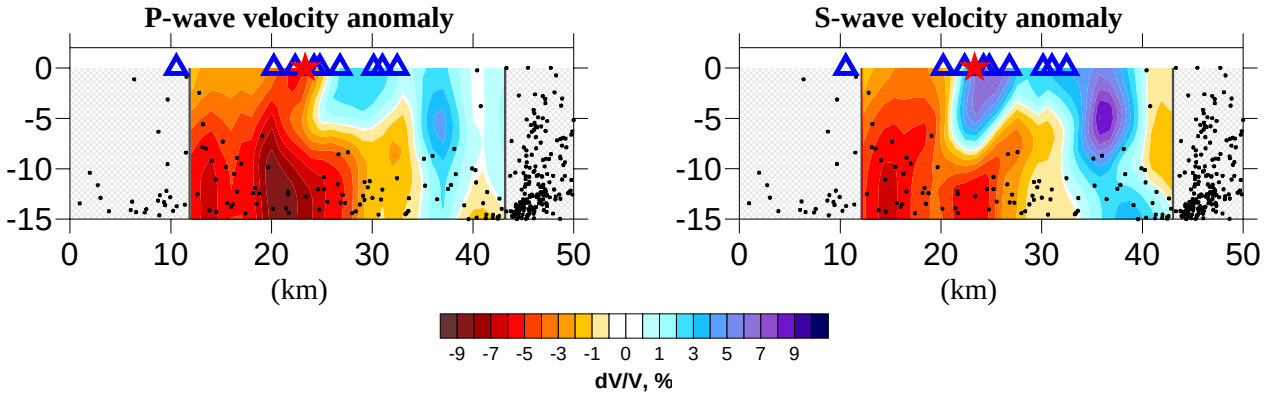

Figure 9. *A vertical west-east tomographic section (line 7 in* ***Fig. 8****) crossing the position of the hot springs, which is marked by a red star. Blue triangles indicate positions of stations projected into the vertical plane. Black dots mark neighbouring hypocenter locations projected into the vertical plane.*

In relation to the geochemical results, it is conceivable that the deep and broad low-velocity region in the crust may be related to a relatively hot magmatic body that is the heat source for the hot springs. Relatively hot material also appears at shallower depth in localized areas to the west and east of the Rwenzori range, with the largest anomaly to the west of the hot springs. It seems plausible that water is heated at depth and rises to the surface through an existing fault or fracture zone, which corresponds to the boundary between fast and slow velocity regions. Currently, this zone seems to be void of any seismic activity. Note, however, that there is a general difficulty to separate the effects of temperature-related velocity reductions from those related to possible changes in rock type (i.e. the sedimentary fill in this graben region).

Absolute velocities are difficult to estimate from tomographic inversions, as true maximum amplitudes of the anomalies are usually underestimated. Furthermore, the temperature effect of a magmatic intrusion on P- and S-wave velocities is difficult to derive. After Kern (1978) and Landolt-Börnstein (1982) the velocity reduction may be estimated to about 0.1 km/s per 100°C. In the tomographic inversion given here, a 10 % anomaly corresponds to about 0.7 km/s change in P-wave velocity and 0.4 km/s change in S-wave velocity. From the low-velocity anomaly observed beneath the hot springs one may estimate that temperatures of more than 1000° in excess temperature are found at depths greater than about 7 km.

References

Lienert, B.R.E., Berg, E. & Frazer, L.N. (1986). Hyocenter: An earthquake location method using centered, scaled, and adaptively least squares. BSSA, Vol. 76, 771-783.

Lienert, B.R.E. & Havskov, J. (1995). A computer program for locating earthquakes both locally and globally. Seismological Research Letters, 66, 26-36.

Kennett, B.L.N. (Ed.) (1991). IASPEI 1991 Seismological Tables. Research School of Earth Sciences, Australian National University.

Kern, H. (1978) The effect of high temperature and high confining pressure on compressional wave velocities in Quartz-bearing and Quartz-free igneous and metamorphic rocks. Tectonophysics, 44, 185-203.

Koulakov, I., & Sobolev, S.V. (2006). Moho depth and three-dimensional P and S structure of the crust and uppermost mantle in the Eastern Mediterranean and Middle East derived from tomographic inversion of local ISC data. Geophysical Journal International, 164, 1, 218-235.

Landolt-Börnstein(1982). Zahlenwerte und Funktionen aus Naturwissenschaft und Technik. Springer Verlag.

Maasha, N. (1975). The Seismicity of the Rwenzori Region in Uganda. Journal of Geophysical Research, 80, No. 11, 1485-1496.

Ochmann, N., Lindenfeld, M., Barbirye, P. & Stadler, C., (2007). Microearthquake survey at the Buranga geothermal prospect, Western Uganda. Proceedings of the 32nd workshop on geothermal reservoir engineering, Stanford University, Stanford, California, January 22-24, SGP-TR-183.

Schlüter, T. (2006). Geological Atlas of Africa, Springer-Verlag Berlin Heidelberg.

Yakovlev A.V., Koulakov, I.Yu. & Tychkov S.A. (2007). Moho depths and three-dimensional velocity structure of the crust and upper mantle beneath the Baikal region, from local tomography. Russian Geology and Geophysics, 48 (2), 204-220.

Author contact details

Prof. Dr. G. Rümpker, Dr. M. Lindenfeld, A. Yakovlev
Facheinheit Geophysik, Institut für Geowissenschaften, J.W. Goethe-Universität Frankfurt, Feldbergstr. 47, 60323 Frankfurt am Main.
Tel.: +49-69-798-24923, Fax: +49-69-798-23280, rumpker@geophysik.uni-frankfurt.de

Appendix: P-wave and S-wave velocity anomalies

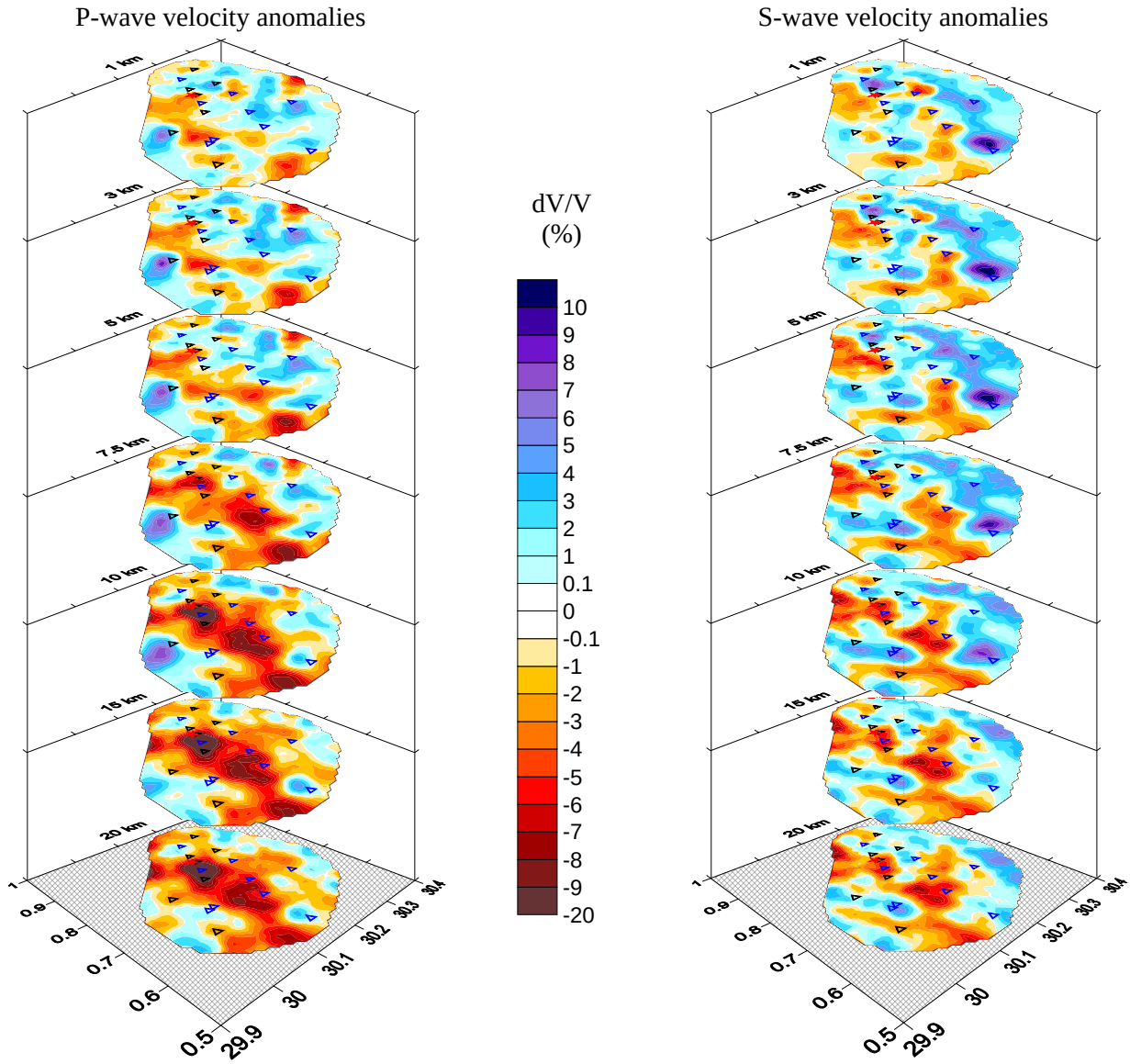

Figure A1. *Horizontal sections of the P- and S-velocity anomalies may in different depth levels of 1, 3, 5, 7.5, 10, 15 and 20 km. Blue (red) colours indicate regions of relatively high (low) velocities with respect to the initial velocity model. A relatively hot magmatic intrusion near the surface is expected to exhibit a negative velocity anomaly.*

P-velocity anomalies

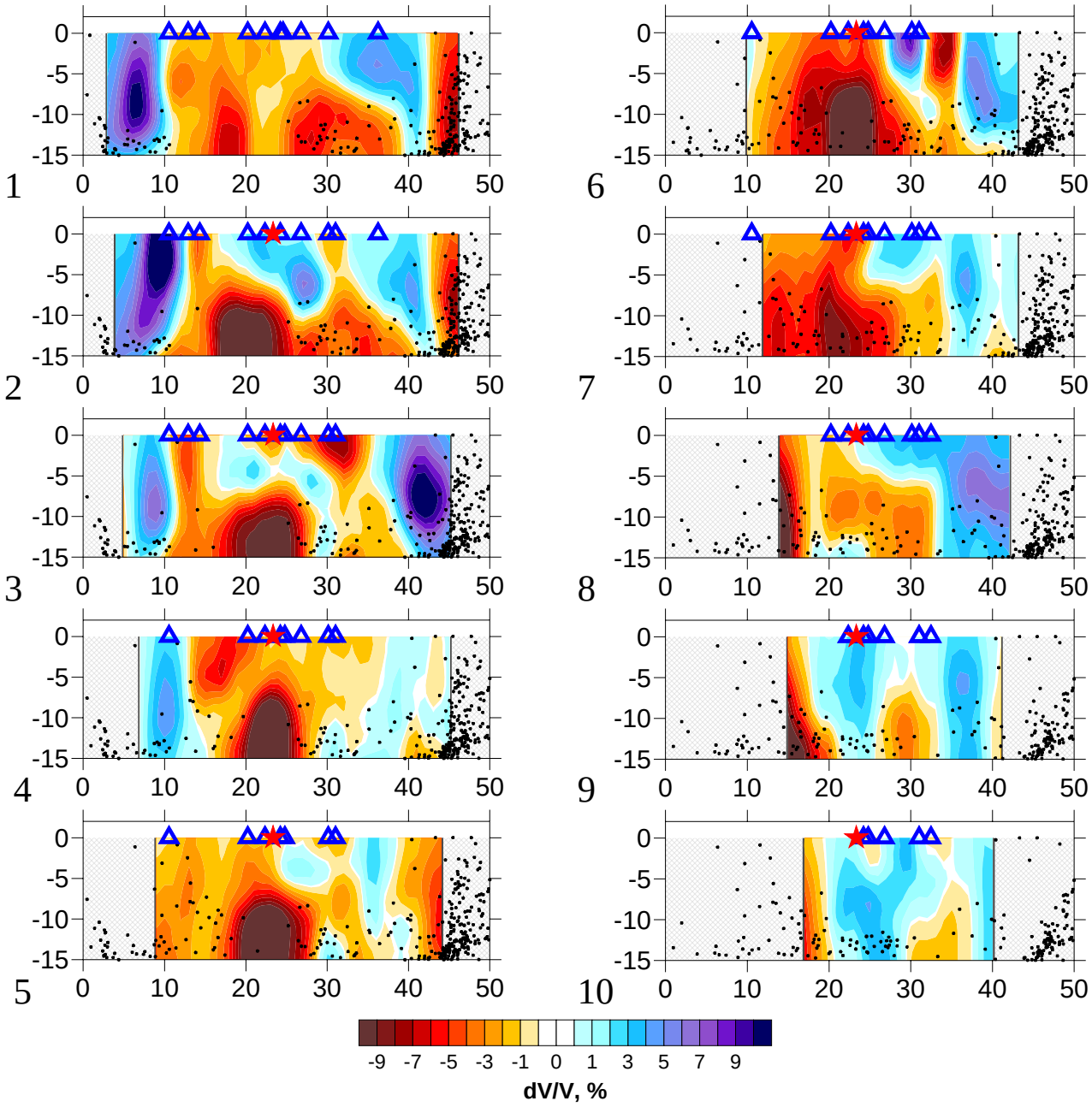

Figure A2a. *Vertical west-east sections of P-velocity anomalies (positions are given in* ***Fig. 8****) near the position of the hot springs, which is marked by a red star. Blue triangles indicate positions of stations projected into the vertical plane. Black dots mark neighbouring hypocenter locations projected into the vertical plane.*

S-velocity anomalies

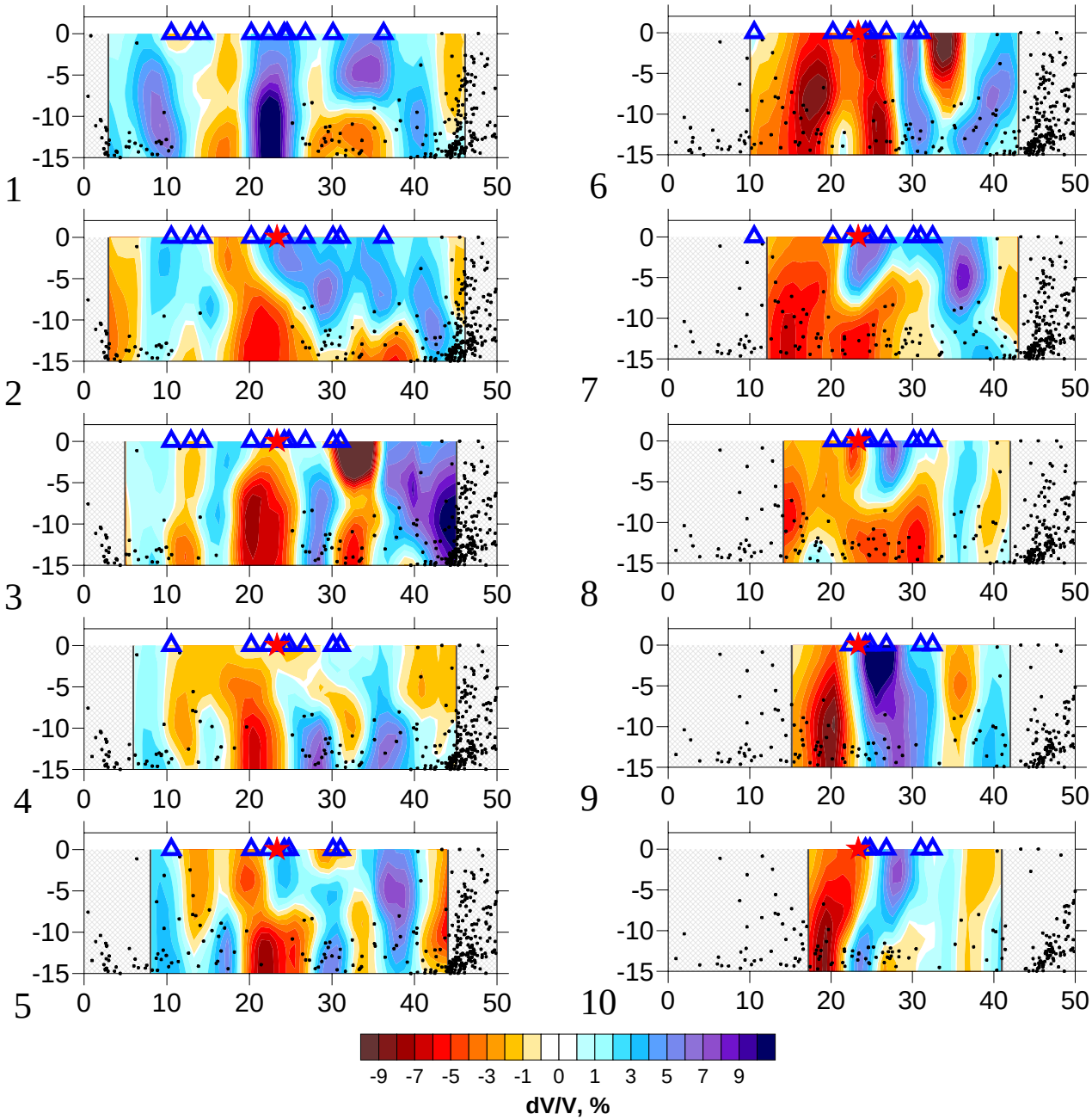

Figure A2b. *Vertical west-east sections of S-velocity anomalies (positions are given in* ***Fig. 8****) near the position of the hot springs, which is marked by a red star. Blue triangles indicate positions of stations projected into the vertical plane. Black dots mark neighbouring hypocenter locations projected into the vertical plane.*

Results of tomographic inversion: depth 1 km

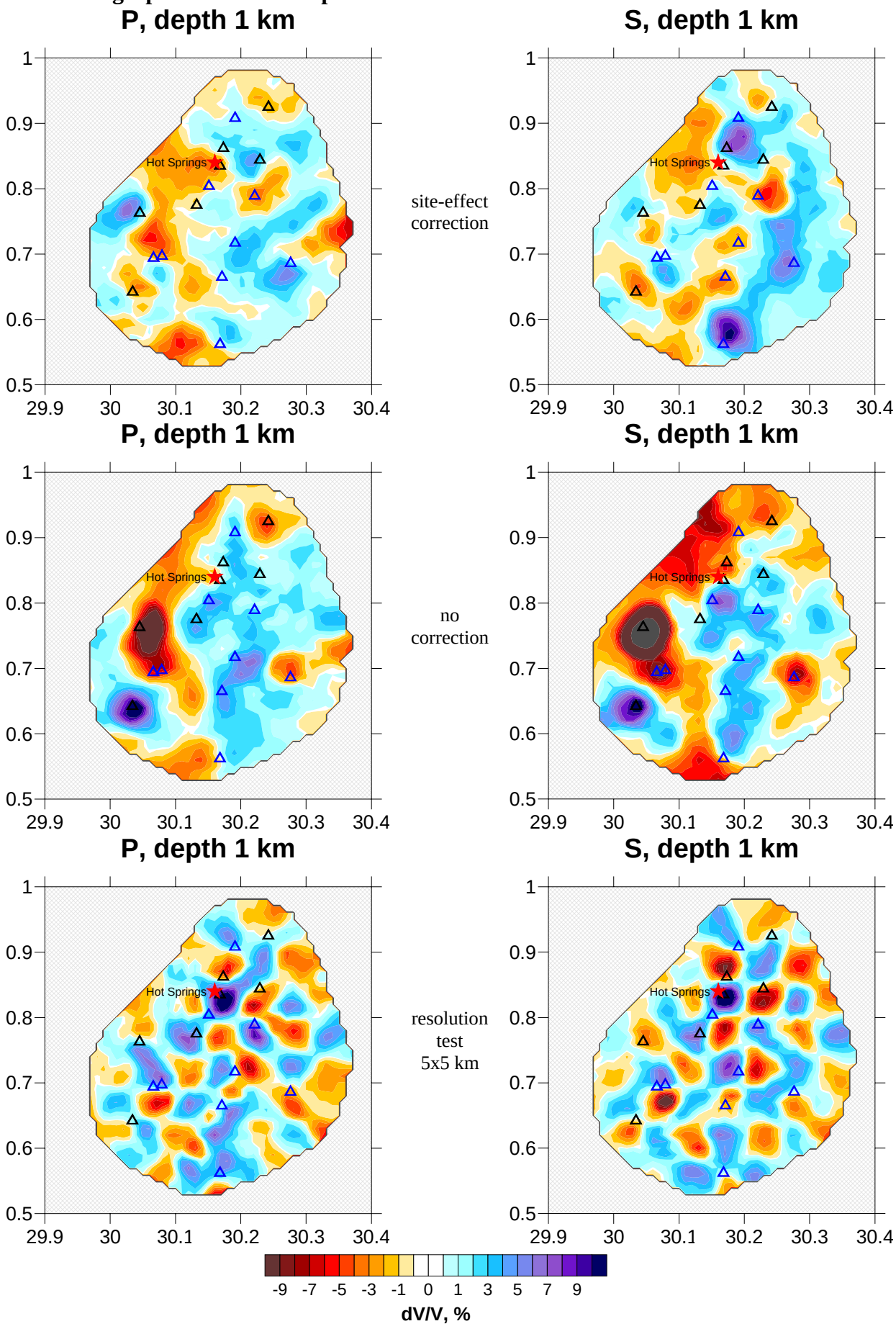

Results of tomographic inversion: depth 3 km

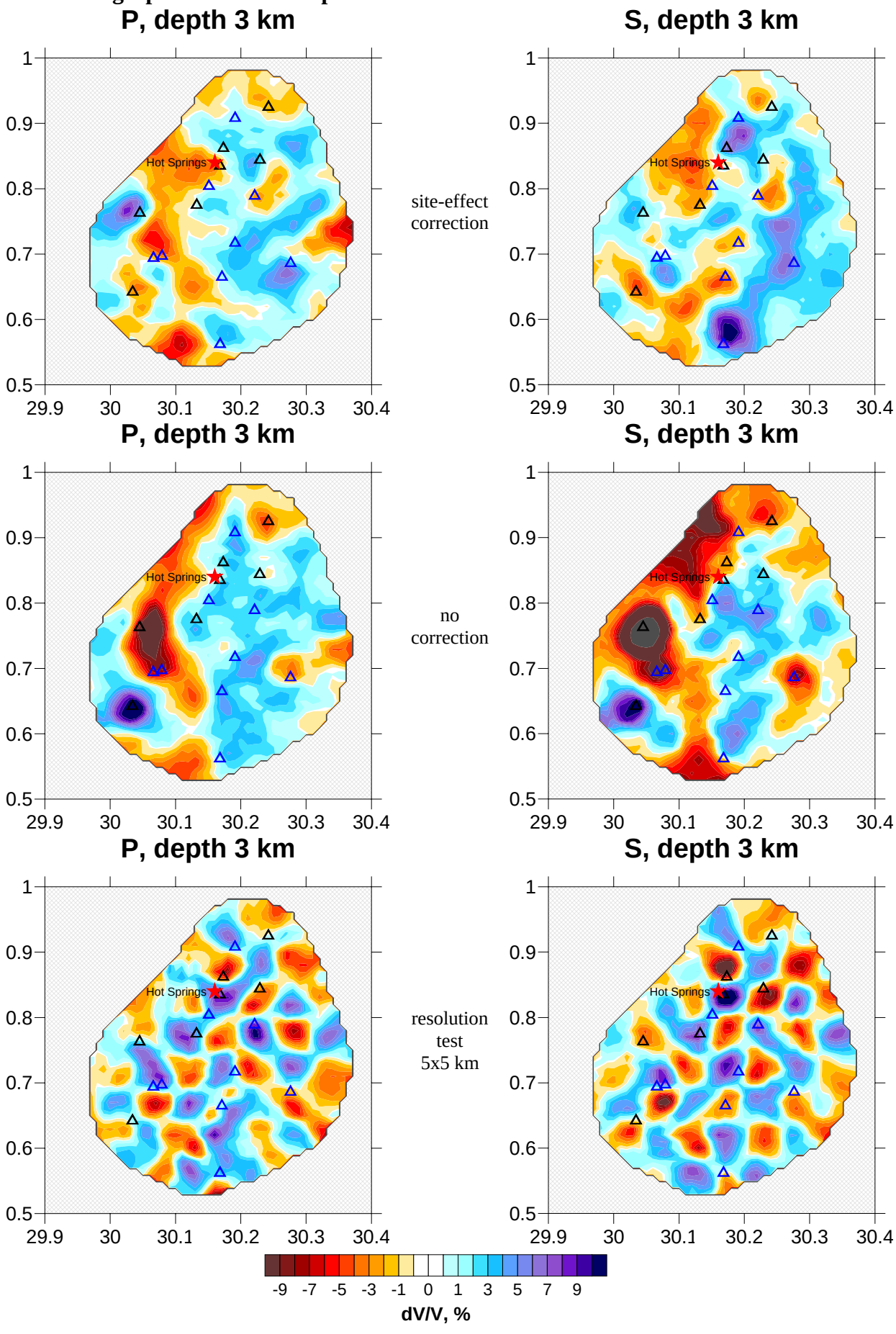

Results of tomographic inversion: depth 5 km

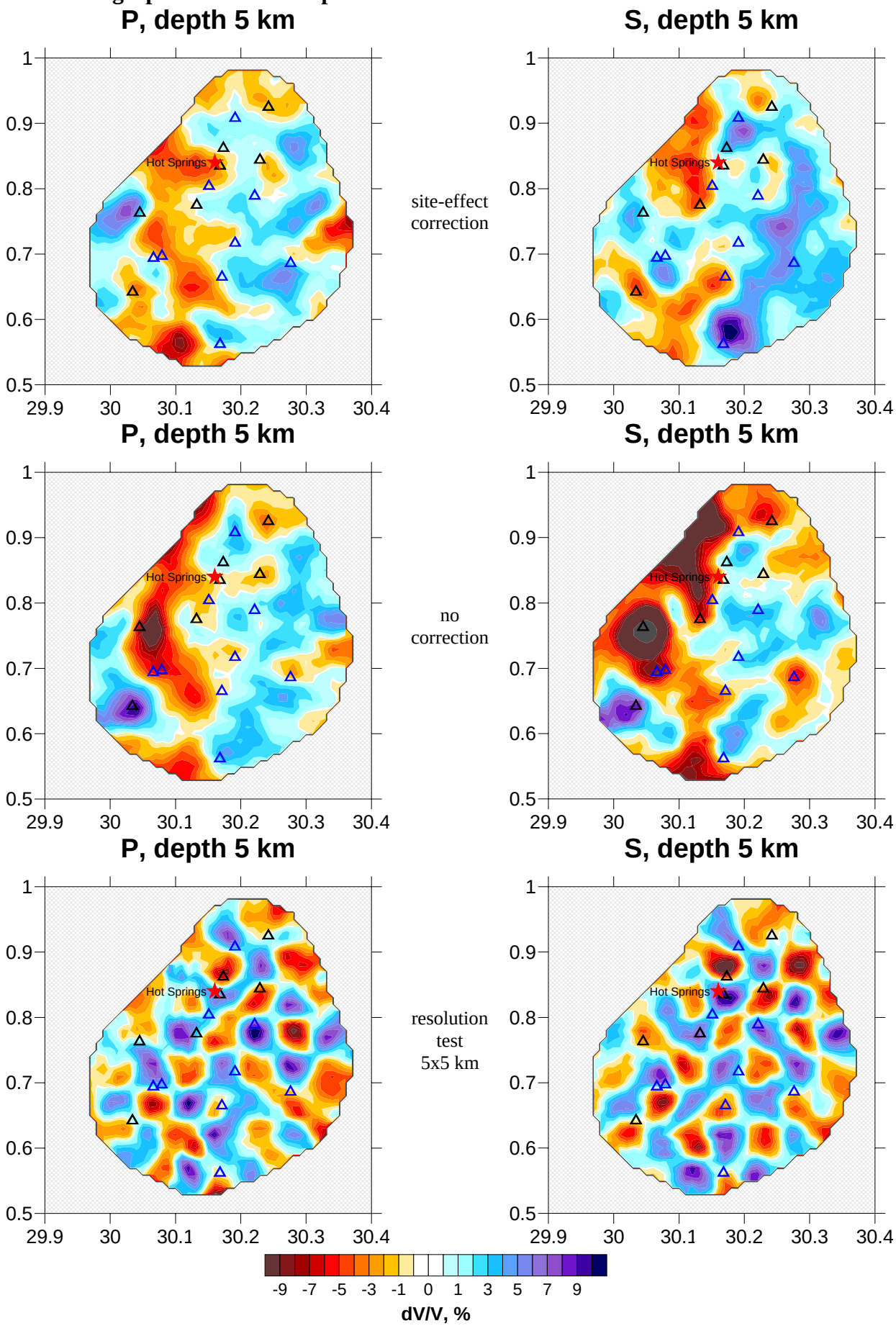

Results of tomographic inversion: depth 7.5 km

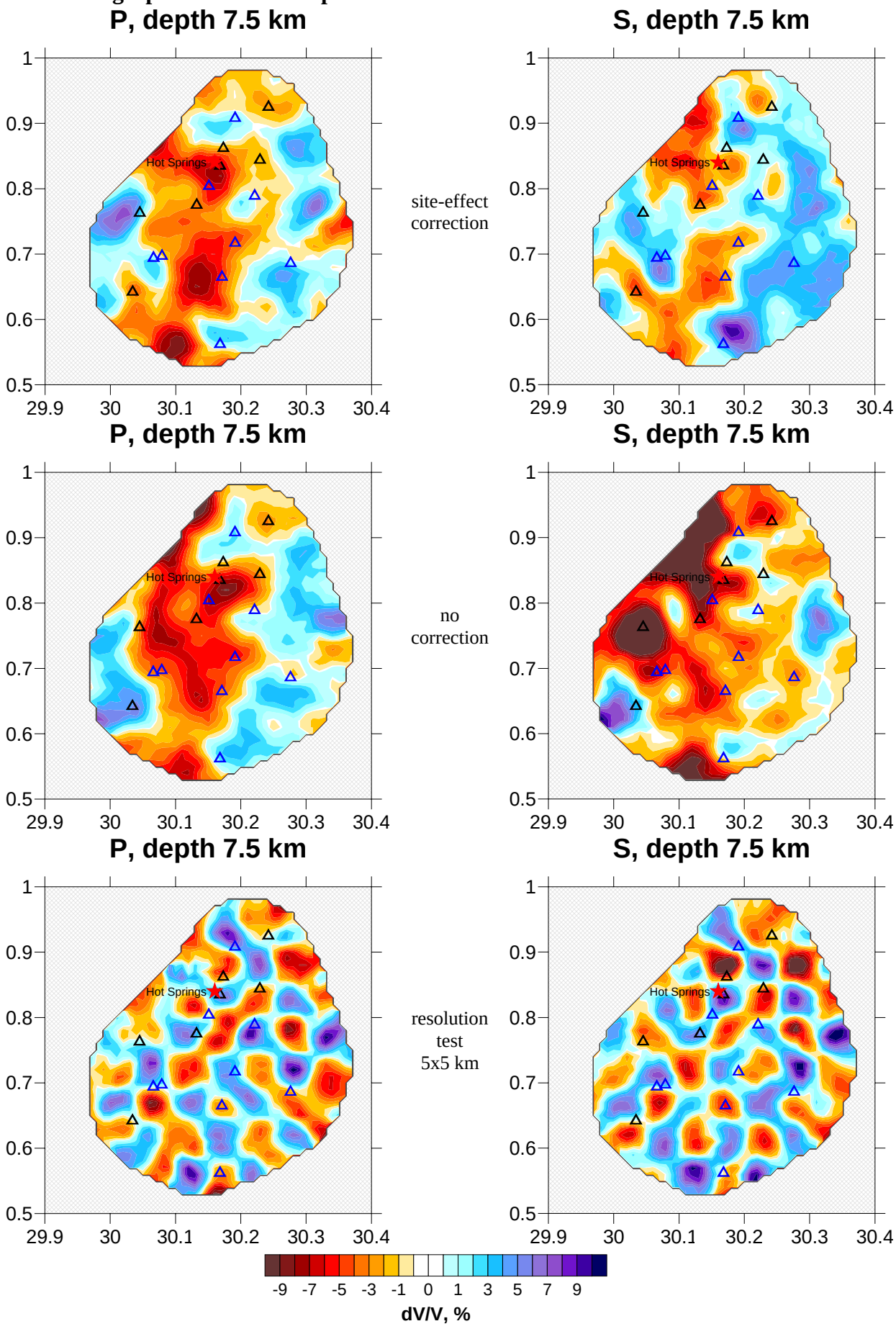

Results of tomographic inversion: depth 10 km

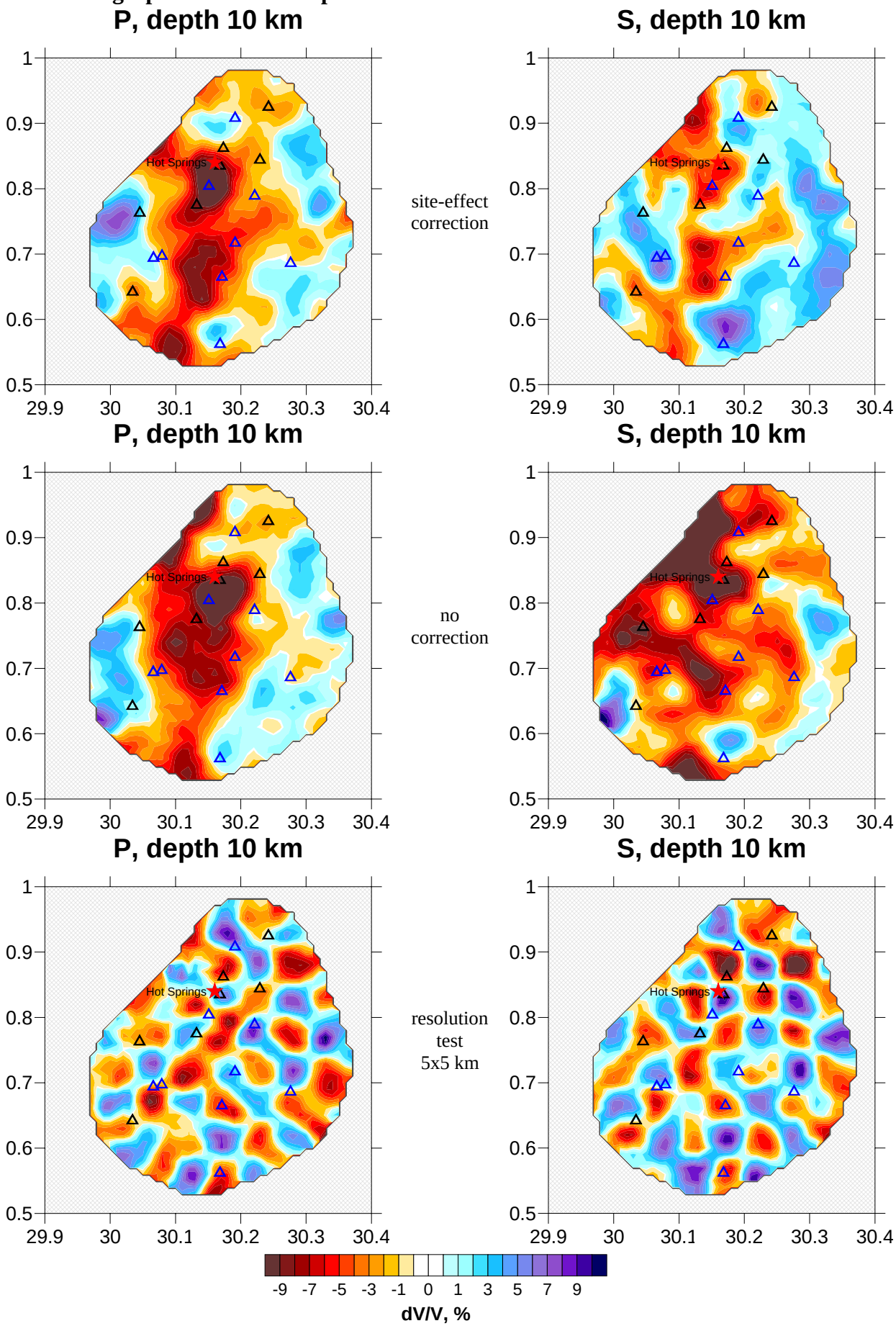

Results of tomographic inversion: depth 15 km

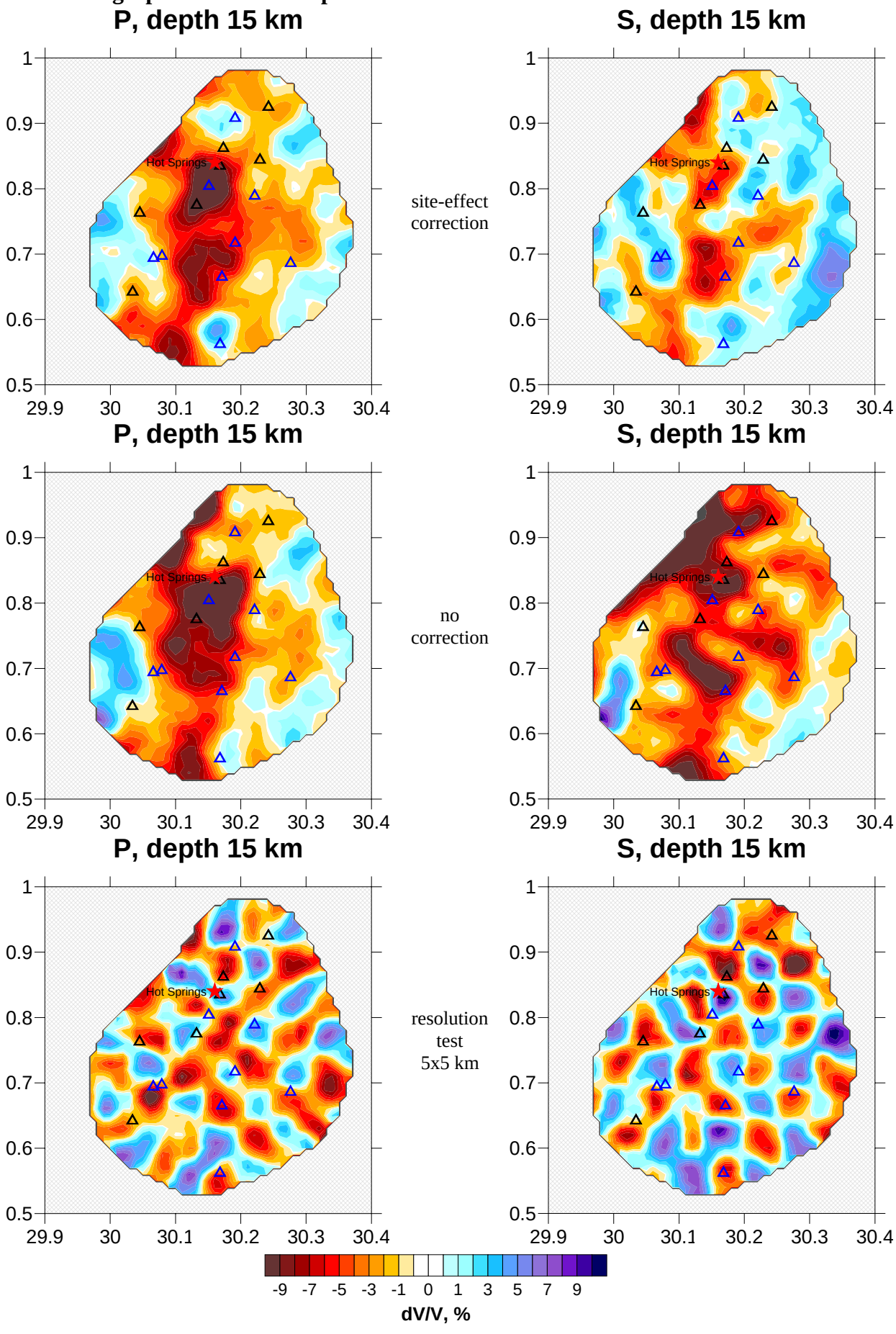

Results of tomographic inversion: depth 20 km